Approximate Maximum Likelihood Estimation Using a 3D GNSS Simulator for Positioning in MP/NLOS Conditions

Nabil Kbayer
TeSA/ISAE-SUPAERO
Toulouse, FRANCE
Email: nabil.kbayer@isae.fr

Mohamed Sahmoudi
and Héctor Ortega
DEOS/ISAE-SUPAERO
Toulouse, FRANCE

Cédric Rouch
French Space Agency (CNES)
Toulouse, FRANCE

Nabil Kbayer is a PhD student at the French Institute of Aeronautics and Space (ISAE-SUPAERO), University of Toulouse, France. He received his engineer degree in signal processing from ISAE-ENSICA. His research interests include signal processing for positioning in challenging environments, multipath and NLOS mitigation and constructive use for cognitive navigation.

Mohamed Sahmoudi received a PhD in signal processing and communications systems from Paris-Sud Orsay University, France, in collaboration with Telecom Paris in 2004. From 2005 to 2007, he was a post-doctoral researcher fellow on GPS Signal Processing and Navigation at Villanova University, PA, USA. In august 2007, he joined the ETS school of engineering at Montreal, Canada, to lead the research team of precise positioning (RTK and PPP). In 2009, he became an Associate Professor at ISAE-SUPAERO, University of Toulouse, France. Currently his research interests focus on all aspects of signal processing for navigation in harsh environment, weak GNSS signals acquisition and tracking, multi-frequency and multi-GNSS receivers, multipath mitigation and constructive use and multi-sensor fusion for robust navigation.

Héctor Ortega is a Telecommunications Engineering student at Telecom BCN (ETSETB), Polytechnic University of Catalonia (UPC), Spain. He is currently carrying out his Final Degree Project at ISAE-SUPAERO. His research interests include signal processing applied to navigation as well as space systems.

Cédric Rouch, graduated in 2013 from the French Civil Aviation University (ENAC) in Toulouse, France. He joined the CNES Navigation and Telecommunications department in 2015. He is involved in GNSS simulation and positioning performance assessment. He is responsible for the development of the SPRING, a software designed for analysis of systems integrating GNSS positioning. He is also in charge of GNSS measurement campaigns and experiments.

Abstract

Recent trends in Global Navigation Satellite System (GNSS) applications in urban environments have led to a proliferation of studies in this field that seek to mitigate the adverse effect of non-line-of-sight (NLOS) phenomena. However, these methods reduce the availability of positioning in deep urban conditions. For such harsh urban settings, this paper proposes a methodology of constructive use of NLOS signals, instead of their elimination. We propose to compensate for the NLOS errors using a 3D GNSS simulator to predict the measurements bias and integrate them as observations in the estimation method. We investigate a novel GNSS positioning technique based on measurement similarity scoring of an array of position candidates. We improve this technique using an estimation of the uncertainty on the bias prediction by 3D modeling. Experiment results using real GNSS data in a deep urban environment confirm the theoretical sub-optimal efficiency of the proposed approach, despite it intensive computational load.

Keywords: *GNSS in urban canyons; Multipath and NLOS reception; Maximum Likelihood Estimation; GNSS simulators*

I. Introduction

A Plethora of land navigation applications benefits from the free accessibility and suitable accuracy of Global Navigation Satellite System (GNSS) for location and timing in urban areas [1]. Motivated by this exponential increase of GNSS based applications in these environments, recent attention has focused on improving positioning accuracy in urban settings. On the one hand, GNSS positioning services are poised to be receiving stringent positioning requirements in cities. On the other hand, these harsh environments present significant challenges for satellite positioning that prevent achieving user requirements.

Actually, the presence of line-of-sight (LOS) blockage deteriorates the positioning accuracy for three reasons. First, it engenders very challenging technical issues for acquiring and tracking the attenuated signals. Hence, the continuity of position estimation cannot be guaranteed if tunnels, tall building and foliage disrupt the GNSS navigation completely. Secondly, the interaction with the environment usually results in the reception of multipath (MP) signals. Besides, if the line of sight (LOS) is blocked and the satellite signal is eventually received through a reflected non-line-of-sight (NLOS) path, the related pseudo-range (PR) measurement will be affected by an additional bias [2]. These combined NLOS and MP biases degrade the position estimation and result in hundreds of meters of positioning error in some situations [3]. Thirdly, blocked satellite signals engender a poor constellation geometry that may affect the Dilution of Precision (DOP) unfavourably which further reduce the positioning accuracy. In view of such technical challenges in urban areas, there is a pressing need for mitigating these unwanted effects to achieve the required positioning accuracy.

This paper is divided into four main sections. The first one proposes a review of the state on the MP/NLOS problem. In the second section, we introduce our contribution for positioning in MP/NLOS conditions. The third section outlines experimental results obtained in an urban canyon in Toulouse using the proposed approach and a 3D GNSS simulator. Finally, some conclusions are summarized in section 4.

II. RELATED WORKS

Broadly speaking, the literature on the NLOS problem falls into three main categories: NLOS identification, NLOS mitigation and NLOS constructive use. The former tends to distinguish between clean LOS signals and NLOS range measurements. Some of the proposed methods investigate the use of additional hardware, allowing this NLOS-LOS distinction. Hardware-based distinction techniques include the use of a dual polarization antenna, a GNSS antenna array and a sky-pointing camera. Without using additional hardware, [4] proposes other indicators of NLOS reception such as elevation angle selection, C/N0-based NLOS detection and inter-satellite consistency checking [5]. MP/NLOS measurements, once identified, can be either discarded [6], down-weighted [7] or used constructively to improve positioning performances [8].

The second approach typically tends to reduce the adverse impact of deteriorated NLOS signals on the estimation accuracy. A number of classical techniques for MP/NLOS mitigation exist in the literature and represent standard features of professional grade GNSS receivers, in particularly those based on narrow and double-delta correlators [9]. In-receiver MP mitigation methods include strobe correlator [10], the Multipath Estimating Delay Lock Loop (MEDLL) [11] and Fast Iterative Maximum-Likelihood Algorithm (FILMA) [12]. However, these in-receiver techniques do not bring a considerable enhancement in case of NLOS reception due to the absence of a LOS signal. Other scientific studies have been carried out for NLOS mitigation at the level of antenna and hardware design, receiver, post-receiver [13], by robust estimation [14], [15], MP modeling [16] or by hybridizations with other external sensors [17].

To deal with the lack of GNSS signals redundancy in urban environments, a new trend of techniques attempt to detect these degraded measurements and use them constructively [8], [18], [19]. In fact, under the poor conditions of satellite visibility, we would like to use constructively these degraded NLOS observables. The idea behind this methodology is to use all available signals in harsh areas since most GNSS signals are prone to reflections in these environments. Discarding degraded GNSS signals will often induce less signal availability which unable to cater continuous navigation throughout the operation.

New trends of methods aim to use constructively degraded measurements by exploiting the measurements model via aiding information about the geometric environment of reception from 3D city models, as in [8], [20]. However, to deal with the problem of the vicinity of the input point provided to the 3D simulator and the unknown position to be estimated, some studies predict the path delay of the NLOS signals across an array of candidate positions [18], [20], [21], [22], i.e. considering signal reception at multiple candidate positions. The positioning technique is then based on scoring position hypotheses by comparison between observations at the receiver and information provided by the 3D model/3D simulator such as the sky visibility [20], the NLOS signal delay [21], the PR measurements [22], [23]. Others approaches combine a simplified 3D model, called urban trench, with a probabilistic method to enhance performances [24].

Another way of exploiting the 3D city model is to predict the NLOS bias via GNSS propagation simulations and then correcting it in the PR measurements [8], [18]. We use a 3D model jointly with a GNSS simulator to characterize on-the-fly the measurements errors in urban environments and to predict blockage and reflection of GNSS signals. With an initial position input, these GNSS simulators simulate the GNSS propagation in a representative type of environment (e.g. open sky, urban and deep urban) and provide the user with several types of information, such as the number and the characteristics of reflections, additional PR biases, etc. The quality and reliability of the simulated signals depends on how close the a priori input position is to the true position and on the reliability of the propagation modeling at the ray-tracing level. In [8] and [18], we have used the 3D model to predict PR errors and use it constructively on the estimation step. We have used these bias predictions in different ways, including instantaneous corrections, using the mean and variance, and other statistics such as the minimum and maximum bounds as constraints in the estimation process.

In [18], we propose a positioning algorithm, called the range bias correction (RBC-3D), based on correcting degraded measurements using information provided by a 3D GNSS simulator. The RBC-3D estimator is based on finding upper and lower bounds of NLOS biases and performing a range bias correction, in the measurements domain, using these predicted PR bias bounds to compute a new position with corrected PR measurements. 3D-mapping measurements correction is therefore performed using a 3D GNSS simulator, able to estimate the PR ranging errors and then correct them.

This PR correction step is a sensitive task: poor PR bias predictions may engender an erroneous ranging correction and then may sensitively reduce the position estimation instead of enhancing it [25]. Besides, unless the search area is small, these approaches are generally computationally intensive. The performances of the PR measurements-based-correction method are strongly linked to the performances of PR bias estimations. One of the greatest challenges is that generally these biases are environment-dependent and highly time-varying and hence very difficult to be estimated.

In this study, we use the 3D GNSS Simulator SPRING to estimate these ranging errors. These estimated biases are then used to define an approximate maximum likelihood estimate. This estimate, called AML-3D, compute a likelihood function over an array of position hypothesis based on the similarity between measured and predicted range information. The proposed estimator produces then an estimation of the final solution over an array of candidate in the position domain. In this work, we use the 3D GNSS simulator SPRING [26], provided by the French Space Agency (CNES), to predict PR errors in urban areas. Experimental results show that better performance can be obtained by using the AML-3D even in harsh environment with mixed MP and NLOS receptions.

III. PROPOSED POSITIONING ALGORITHM

A. Effect of MP/NLOS biases on Position estimation

GNSS is a global technology that allows users over the globe to locate themselves to navigate and have a mean for synchronization on a common time reference. The user position is provided by a dedicated GNSS device able to estimate the time of travel of emitted signals along line-of-sight (LOS) paths from at least four GNSS satellites. However, signal obstruction and degradation are more prominent in harsh environments as opposed to open sky environments, inducing then an additional MP/NLOS ranging bias. Considering N emitting GNSS satellites, the following linearized equation formulates the satellite positioning problem at each time step [27]:

$$\mathbf{y} = \mathbf{H_0}\mathbf{x} + \mathbf{v} + \mathbf{b} \tag{1}$$

Where, throughout this paper, the $[M, 1]$ state vector $\mathbf{x} = (x - x_0, y - y_0, z - z_0, b_{Rx})^\top$ contains the parameters of primary interest, i.e. the three coordinates of the user position $(x, y, z)^\top$ and the receiver clock bias b_{Rx}, which is common between all the received satellites. It is important to note that the first three parameters in the unknown $\mathbf{x}$ to be estimated represent an incremental deviation from the known reference point $\mathbf{x_0} = (x_0, y_0, z_0)^T$ about which the linearization took place. $\mathbf{y} = (y_1, \cdots, y_N)^\top$ is the $[N, 1]$ linearised pseudorange (PR) measurements vector, or PR innovation around a reference location $\mathbf{x_0}$. $\mathbf{H} = (\frac{\partial h_1(\mathbf{x_0})}{\partial \mathbf{x}}, \cdots, \frac{\partial h_N(\mathbf{x_0})}{\partial \mathbf{x}})^\top$ contains the unit line-of-sight (LOS) vectors between the satellites and the previous user position $\mathbf{x_0}$. This matrix describes the linear connection between the measurements $\mathbf{y}$ and the unknowns $\mathbf{x}$. $\mathbf{b} = (b_1, \cdots, b_N)^\top$refers to the additional measurement bias caused by MP/NLOS receptions $[N, 1]$ and is commonly called PR bias. $\mathbf{v} = (v_1, \cdots, v_N)^\top$ is the measurement noise supposed to be a white Gaussian noise characterized by a known covariance matrix $\mathbf{R} = E\{\mathbf{v}\mathbf{v}^\top\}$.

The likelihood cost function for user position estimation is straightforward [28]:

$$J(\mathbf{y}|\mathbf{x}, \mathbf{b}) = \|\mathbf{y} - \mathbf{H}_0\mathbf{x} - \mathbf{b}\|^2_{\mathbf{R}^{-1}} = (\mathbf{y} - \mathbf{H}_0\mathbf{x} - \mathbf{b})^\top \mathbf{R}^{-1}(\mathbf{y} - \mathbf{H}_0\mathbf{x} - \mathbf{b}) \tag{2}$$

The maximum likelihood estimate (ML) is the estimate that minimizes the above likelihood cost function as:

$$\hat{\mathbf{x}}_{ML} = \underset{\mathbf{x}}{\operatorname{argmin}}\, J(\mathbf{y}|\mathbf{x}, \mathbf{b}) = \mathbf{H}_0^+(\mathbf{y} - \mathbf{b}) \tag{3}$$

where $\mathbf{H}_0^+ = (\mathbf{H}^\top\mathbf{R}^{-1}\mathbf{H})^{-1}\mathbf{H}^\top\mathbf{R}^{-1}$ is the pseudo-inverse of $\mathbf{H}_0$ weighted by the inverse of the measurements covariance matrix $\mathbf{R}$. The mean square error (MSE) of this estimator can be expressed as:

$$MSE[\hat{\mathbf{x}}_{ML}] = E\{(\hat{\mathbf{x}}_{ML} - \mathbf{x})(\hat{\mathbf{x}}_{ML} - \mathbf{x})^\top\} = E\{\mathbf{H}_0^+\mathbf{n}(\mathbf{H}_0^+\mathbf{n})^T\} = \mathbf{H}_0^+E\{\mathbf{n}\mathbf{n}^T\}(\mathbf{H}_0^+)^T = (\mathbf{H}_0^\top\mathbf{R}^{-1}\mathbf{H}_0)^{-1} \tag{4}$$

The ML estimate can be seen also as a least squares solution applied on corrected ranging measurements: a sum of a bias free-estimate $\mathbf{H}_0^+\mathbf{y}$, i.e. computed as if no additional bias were present, and a bias-correction term $\mathbf{H}_0^+\mathbf{b}$.

In general, the bias-correction term cannot be computed since the MP/ NLOS is unknown, highly variable and hard to be estimated. Thus, the ML computation is impossible and only a bias free-estimate can be performed. This bias free-estimate is equal to the least squares estimator (LS) of problem (1). This estimator is less efficient than the optimal ML estimate. Indeed, we have the following inequality satisfied by the overall mean square error OMSE (trace of the MSE matrix):

$$OMSE[\hat{\mathbf{x}}_{LS}] = \mathrm{Tr}\{(\mathbf{H}_0^\top\mathbf{R}^{-1}\mathbf{H}_0)^{-1}\} + \mathrm{Tr}\{\mathbf{H}_0^+E\{\mathbf{b}\mathbf{b}^\top\}(\mathbf{H}_0^+)^\top\} \geq \mathrm{Tr}\{(\mathbf{H}_0^\top\mathbf{R}^{-1}\mathbf{H}_0)^{-1}\} = OMSE[\hat{\mathbf{x}}_{ML}] \tag{5}$$

B. Approximate Maximum Likelihood estimate (AML-3D)

Since the computation of the likelihood cost function (2) is theoretically impossible without any prior information on the PR bias, we propose a new cost function that approximates the theoretical maximum-likelihood cost function. To do that, we make use of the 3D GNSS simulator SPRING.

First of all, we distinguish between two kinds of 3D models: ones providing pure geometrical information on the building and street sizes [20] and others combined with 3D GNSS simulators. The latter are more informative and provide users with simulated GNSS signals at any input position and time using Ray-Tracing techniques [26]. This second kind of cited 3D models are used jointly with a 3D GNSS simulator in order to characterize on-the-fly measurement errors in urban environments. It is evident that the predicted bias and errors from the 3D propagation model cannot be instantaneous and accurate. The quality and reliability of the PR bias estimation depends on many factors such as the accuracy of signal propagation modeling, the precision of 3D city modeling, receiver setting, etc...

In this study, we use the 3D GNSS Simulator SPRING to estimate these ranging errors. We start by defining a search area in the environment under study. Within this search area, we set up an array of candidate positions $\Gamma = \{\mathbf{x}_i = (x_i, y_i, z_i, b_{Rx})^\top\}$ with a defined spacing. Providing an input position and a GNSS time, the 3D simulator SPRING is used to predict the corresponding PR biases for each received ranging measurement, i.e. for this grid of candidate positions $\Omega = \{\mathbf{b}_{3D}(\mathbf{x}_i) =$

$(\mathbf{b}_{3D}(\mathbf{x}_i)_1, \cdots, \mathbf{b}_{3D}(\mathbf{x}_i)_N)^\top\}$, we estimate a bank of MP/NLOS bias vectors. Finally, we define the approximate maximum-likelihood cost function as:

$$\begin{aligned} \Pi : \Gamma &\rightarrow \mathbb{R} \\ \mathbf{x}_i &\mapsto \Pi(\mathbf{y}|\mathbf{x}_i, \mathbf{b}_{3D}(\mathbf{x}_i)) = \|\mathbf{y} - \mathbf{H}_0\mathbf{x}_i - \mathbf{b}_{3D}(\mathbf{x}_i)\|^2_{\mathbf{R}^{-1}} \end{aligned} \tag{6}$$

By evaluating this score function on the array of candidate positions, we define an approximate maximum likelihood (AML) estimator as:

$$\hat{\mathbf{x}}_{AML} = \underset{\mathbf{x}_i}{\operatorname{argmin}}\, \Pi(\mathbf{y}|\mathbf{x}_i, \mathbf{b}_{3D}(\mathbf{x}_i)) \tag{7}$$

This AML estimator represents the candidate position that minimizes likelihood scores (approximate maximum-likelihood function) for the set of candidate positions. In this sub-section, we will derive some properties on AML estimator $\hat{\mathbf{x}}_{AML}$ and cost function that demonstrate the convergence of this estimator to the ML estimator over some conditions. Since the bias estimation by 3D simulations cannot be accurate, we define the uncertainty on the bias estimation as:

$$\delta_{3D} = \|\mathbf{b} - \mathbf{b}_{3D}(\mathbf{x})\|^2_{\mathbf{R}^{-1}} \tag{8}$$

1) Lemma 1:Convergence of cost function to maximum-likelihood cost function:: if we consider $\eta \ll 1$, then:

$$|\min_{\mathbf{x}_i} \Pi(\mathbf{y}|\mathbf{x}_i, \mathbf{b}_{3D}(\mathbf{x}_i)) - \min_{\mathbf{x}_i} J(\mathbf{y}|\mathbf{x}_i, \mathbf{b})| \leq (1+\eta)\delta_{3D} \tag{9}$$

Proof:
Using the reverse triangle inequality, the difference between the two cost functions can be increased by:

$$|\Pi(\mathbf{y}|\mathbf{x}_i, \mathbf{b}_{3D}(\mathbf{x}_i)) - J(\mathbf{y}|\mathbf{x}_i, \mathbf{b})| \leq \|[\mathbf{y} - \mathbf{H}_0\mathbf{x}_i - \mathbf{b}_{3D}(\mathbf{x}_i)] - [\mathbf{y} - \mathbf{H}_0\mathbf{x}_i - \mathbf{b}]\|^2_{\mathbf{R}^{-1}}$$

It follows:

$$|\Pi(\mathbf{y}|\mathbf{x}_i, \mathbf{b}_{3D}(\mathbf{x}_i)) - J(\mathbf{y}|\mathbf{x}_i, \mathbf{b})| \leq \|[\mathbf{b} - \mathbf{b}_{3D}(\mathbf{x}_i])\|^2_{\mathbf{R}^{-1}}$$

Using the following inequality:

$$\|\mathbf{b} - \mathbf{b}_{3D}(\mathbf{x}_i)\|^2_{\mathbf{R}^{-1}} \leq \|\mathbf{b} - \mathbf{b}_{3D}(\mathbf{x})\|^2_{\mathbf{R}^{-1}} + \|\mathbf{b}_{3D}(\mathbf{x}) - \mathbf{b}_{3D}(\mathbf{x}_i)\|^2_{\mathbf{R}^{-1}}$$

We can conclude that:

$$|\min_{\mathbf{x}_i} \Pi(\mathbf{y}|\mathbf{x}_i, \mathbf{b}_{3D}(\mathbf{x}_i)) - \min_{\mathbf{x}_i} J(\mathbf{y}|\mathbf{x}_i, \mathbf{b})| \leq \delta_{3D} + \min_{\mathbf{x}_i} \|\mathbf{b}_{3D}(\mathbf{x}) - \mathbf{b}_{3D}(\mathbf{x}_i)\|^2_{\mathbf{R}^{-1}}$$

If the array of candidate positions is wisely chosen, the true position will be close or among the considered grid of candidate positions and hence we will get:

$$\min_{\mathbf{x}_i} \|\mathbf{b}_{3D}(\mathbf{x}) - \mathbf{b}_{3D}(\mathbf{x}_i)\|^2_{\mathbf{R}^{-1}} \leq \eta\delta_{3D}$$

This proves lemma 1. This lemma shows that, conditioned by 3D GNSS simulator accuracy, the minimum of the approximate maximum-likelihood cost function Π converges to the minimum of the maximum-likelihood cost function J.

2) Lemma 2: Convergence of AML estimator to true position::

$$\mathrm{Tr}\{MSE(\hat{\mathbf{x}}_{AML})\} \underset{\delta_{3D}\to 0}{\longrightarrow} \mathrm{Tr}\{MSE(\hat{\mathbf{x}}_{ML})\} \tag{10}$$

Proof: See Appendix A.

Lemma 2 demonstrates that, conditioned by 3D GNSS simulator accuracy, the overall mean square error (trace of the MSE matrix) of the AML estimator converges to the minimum overall mean square error of the ML solution of problem (1).

3) Lemma 3: Convergence of AML estimator to ML estimator:: If we suppose that all the diagonal values of the covariance matrix are equals, i.e $\mathbf{R} = \sigma\mathbf{I}$, then we have:

$$\|\hat{\mathbf{x}}_{AML} - \hat{\mathbf{x}}_{ML}\|^2_2 \leq \frac{N \times GDOP}{\sigma^2}(1+\eta)\delta_{3D} \tag{11}$$

where $GDOP$ is the Geometric Dilution Of Precision, N is the number of received GNSS signals and $\eta \ll 1$.

Proof: See Appendix B.

Lemma 3 proves that, conditioned by 3D GNSS simulator accuracy, the AML estimator converges to the ML estimator, i.e. if the 3D GNSS simulator is so accurate, the AML will converge to the ML estimator which is the Minimum Variance Unbiased Estimator (MVUE) of the problem (1).

C. Practical Implementation

1) Scoring Function Computation:

Even if it has been proven that the AML estimator converges to the most efficient ML estimator under the assumption of an accurate 3D simulation, the expression of such estimator is very computationally intensive since it requires a research over a grid of candidate position containing four unknowns. These unknowns are the user position (x, y, z) and the clock bias b_{Rx} (common between all the received satellites).

To reduce the estimation complexity, a classical hypothesis consists of using the 3D GNSS simulator to avoid the estimation of the height information. Given the horizontal coordinates of each grid point, a height is associated to this point using the 3D city model which avoids the computational load over a 3D search area.

For the sake of simplification, the receiver clock bias is eliminated by proceeding to a differentiation of all ranging measurements across satellites using a reference satellite. The selection of reference satellite is quite important. This satellite must have a reliable and almost clean ranging measurement. Basic indicators for this selection process include elevation angle and C/N0 values. Ref. [29] proposes a reference satellite selection using LOS probability obtained via signal power distributions and experimental data.

Since the proposed approach is 3D-simulation-accuracy-dependent, we propose to estimate the uncertainty on bias estimation provided by the 3D GNSS simulator. Preliminary tests on the evaluation of the performance of this tool show that PR biases of high elevation signals are usually correctly estimated, as the signal have less interactions with the environment surrounding the receiver contrary to low or medium elevation signals. Then, we propose the following formula as estimation for this uncertainty on bias prediction. $\alpha_{Max-Inaccuracy}$ refers to the highest error on bias estimation.

$$\tilde{\delta}_{3D} = \alpha_{Max-Inaccuracy} \exp(\mathbf{Elev}/(\mathbf{Elev} - 90)) \tag{12}$$

where $\mathbf{Elev}$ refers to satellite elevation angle in degrees. Similarly, we can also estimate this uncertainty on bias prediction based on the C/N0 ratio as:

$$\tilde{\delta}_{3D} = \alpha_{Max-Inaccuracy} 10^{\frac{C/N0}{C/N0_{Max}}} \tag{13}$$

Once a reference satellite is selected, we modify the approximate maximum-likelihood cost function (6) as follows:

$$\tilde{\Pi}(\mathbf{y}|\mathbf{x}_i) = \|\mathbf{y} - y_{ref} - (\mathbf{H}_0 - \mathbf{H}_0(ref,:))\mathbf{x}_i - \mathbf{b}_{3D}(\mathbf{x}_i) - \tilde{\delta}_{3D}\|^2_{\mathbf{R}^{-1}} \tag{14}$$

where y_{ref} is the ranging measurement of the reference satellite and $\mathbf{H}_0(ref,:)$ is the row of matrix $\mathbf{H}_0$ corresponding to the reference satellite. The array of candidate positions is now an array of 2D points $\Gamma = \{\mathbf{x}_i = (x_i, y_i, z)^\top\}$, where the height z is computed using terrain height aiding via the 3D simulator.

2) Final Position Estimation:

Considering the final position as the candidate position having the lowest score, i.e. minimizing the approximate maximum-likelihood cost function in (14), is risky. Therefore, we propose to estimate the final AML-3D solution as a weighted average of the candidate positions with the lowest scores, i.e. the highest PR measurements matching, as:

$$\hat{\mathbf{x}}_{AML} = \frac{\sum_{i=1}^{N_{Th}} (\tilde{\Pi}(\mathbf{y}|\mathbf{x}_i^{\Omega}) < Th)\mathbf{x}_i^{\Omega}}{\sum_{i=1}^{N_{Th}} (\tilde{\Pi}(\mathbf{y}|\mathbf{x}_i^{\Omega}) < Th)} \tag{15}$$

Where Th is the threshold used for selecting the lowest scores, N_{Th} corresponds to the number of grid points with a matching score lower than the threshold Th and the set $\Omega = \{\mathbf{x}_i^{\Omega}, i = 1, \cdots, N_{Th}\}$ refers to the subset of candidate positions with the lowest scores. Practically, we have fixed Th to the 15th percentile of the values in the approximate maximum-likelihood cost function, i.e. the final AML-3D solution is an average of the 15% of points having a score matching higher than Th.

As a way of illustration, a block diagram of our proposed algorithm is given in Fig. 1. Finally, the proposed approach is summarized in the algorithm 1 below.

IV. EXPERIMENTAL RESULTS

A. General Experimental Setup

To evaluate the proposed solution, a dynamic positioning test was conducted in an urban environment. GPS L1 C/A code PR measurements were collected around Capitole Square in Toulouse using an UBLOX 6T receiver, and a SPAN Novatel system including a DGPS receiver tightly integrated with an IMU-FSAS (from iMAR), both at a rate of 4 Hz. We consider the trajectory provided by the Novatel receiver as the reference trajectory for comparison with our algorithms.

An overview of the considered urban environment and the Sky-plot of the GPS received satellites in the deep urban section are shown in Fig. 2.

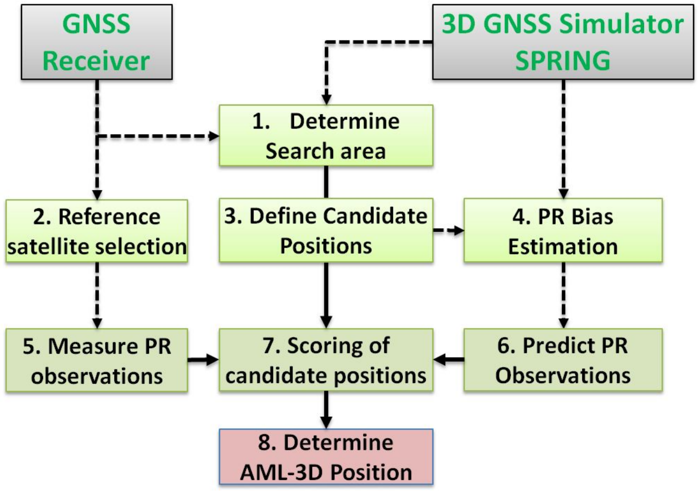

Fig. 1: AML-3D algorithm block diagram

Algorithm 1 AML Estimation

Inputs: $\mathbf{y}, \mathbf{H}_0$ and maybe $\tilde{\delta}_{3D}$

Output: $\hat{\mathbf{x}}_{AML}$

1: **Reference satellite selection using elevation criterion**

2: **Define search area and grid of candidate positions**
Define an array of 2D points $\Gamma = \{\mathbf{x}_i = (x_i, y_i, z)^\top\}$

3: **Estimate a bank of PR biases over candidate positions**
Estimate PR biases, using 3D GNSS simulations, for the considered array of candidate positions
$\Omega = \{\mathbf{b}_{3D}(\mathbf{x}_i) = (\mathbf{b}_{3D}(\mathbf{x}_i)_1, \cdots, \mathbf{b}_{3D}(\mathbf{x}_i)_N)^\top\}$

4: **Likelihood scoring for each candidate position**
Compute $\tilde{\Pi}(\mathbf{y}|\mathbf{x}_i)$ using (14)

5: **AML-3D position estimation**
Estimate AML-3D solution $\hat{\mathbf{x}}_{AML}$ using (15)

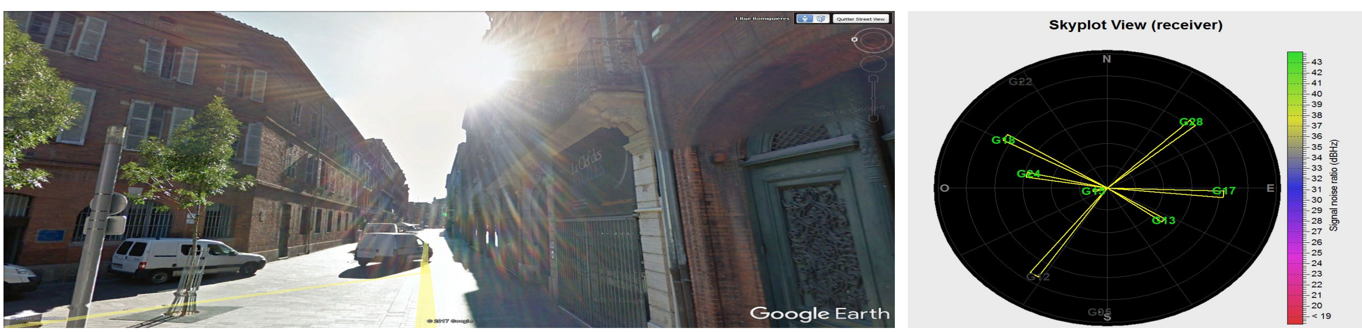

(a) Tested Urban Environment

(b) Sky-plot of GPS satellites

Fig. 2: Overview of experimental setup

For this validation test, we have selected a trajectory along an urban environment characterized by narrow streets and medium-height buildings, which are predominantly the down-towns of European cities. We have used the elevation angle as criterion for reference satellite selection.

For illustration of the used grid of candidate positions, Fig. 3 shows the used array of positions. In this experimental evaluation of our algorithm, we have used 1600 candidate positions in a square area in the region of interest. These positions are uniformly distributed in this search area with a spacing of 1m. A pre-processing algorithm is implemented to exclude the indoor points based on the 3D model of the city. Hence, this grid of candidate positions contains only outdoor locations. The red dots refer to the used reference trajectory, while white dots represent the considered candidate positions.

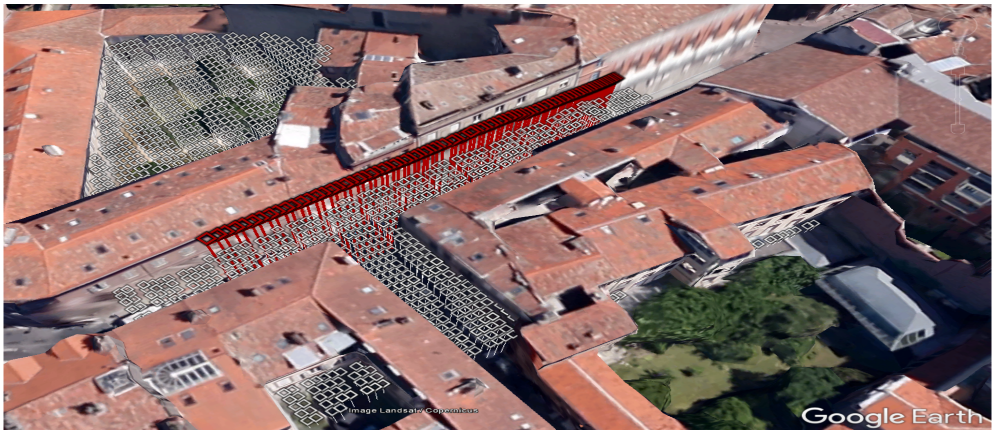

Fig. 3: Used Grid of candidate positions

B. 3D Simulations

For each of these candidate positions, we perform 3D simulation using the 3D GNSS simulator SPRING. The simulator SPRING, provided by the French space agency CNES-Toulouse, is used to estimate the PR bias errors. SPRING is a full software simulator that models the pseudo-range measurements and calculates the PVT solution considering the 3D environment of the receiver antenna. At each time step, the 3D simulation is applied to an input point that allows the calculation and the prediction of the bias error on each received signal at this point.

Fig. 4 shows the 3D simulations of GNSS measurements in one candidate position at a defined GPS time. The main steps used for 3D PR bias estimation at each candidate position are summarized in the algorithm 2 below.

Algorithm 2 3D GNSS Simulation

Inputs: GPS Time, Satellite ephemeris, 3D city Model and candidate position $\mathbf{x}_i$

Output: 3D bias $\mathbf{b}_{3D}(\mathbf{x}_i)$

1: **Compute satellite positions**

2: **Determine LOS distance between each satellite and the candidate position**
For each satellite Sat_i, compute $PR_i^{LOS} = \|\mathbf{x}_i - \mathbf{x}_i^{Sat_i}\|_2$

3: **Predict 3D received PR measurements**
For each satellite Sat_i, predict PR_i^{3D}, using the 3D model, ray-tracing algorithm and the receiver model implemented in SPRING

4: **Compute PR bias**
As all the other ranging errors are not modelled, PR bias is the difference between predicted PR measurements and LOS distance: $[\mathbf{b}_{3D}(\mathbf{x}_i)]_i = PR_i^{3D} - PR_i^{LOS}$

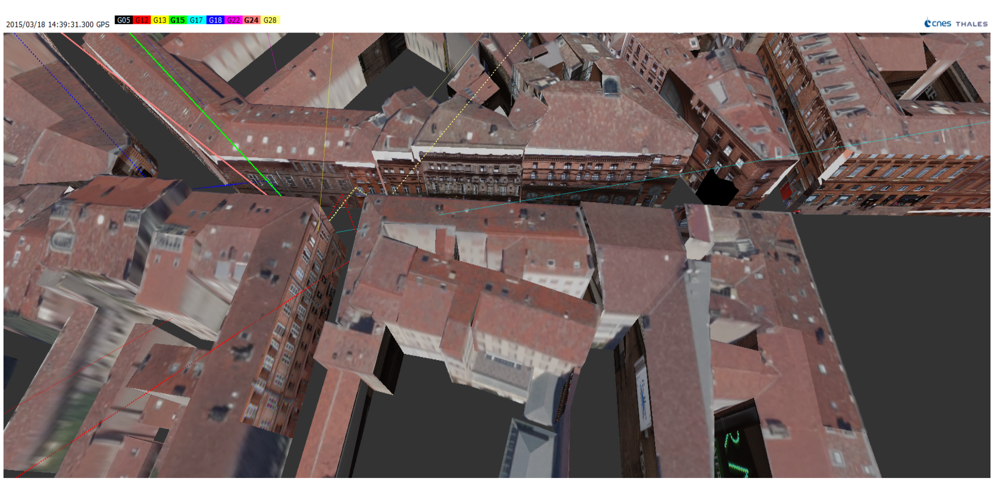

Fig. 4: 3D GNSS Simulation using SPRING

C. Comparison Algorithm

Considered among the most mature 3D model based positioning approaches, Shadow Matching solution [30] use 3D building models to improve cross-track positioning accuracy in harsh environments by predicting which satellites are visible from different candidate locations and comparing this information with the measured satellite visibility to determine the final user solution. This positioning approach is based on GNSS and 3D model fusion for satellite shadows scoring of candidate positions. By achieving metre-order cross-street positioning in urban canyons, it was implemented for smartphone applications [31], [32]. The basic Shadow-Matching approach can summarized in the algorithm 3 below.

Algorithm 3 Shadow-Matching Estimation

Inputs: $\mathbf{y}, \mathbf{H}_0$, C/N0 Coefficients (for satellite visibility)

Output: $\hat{\mathbf{x}}_{SM}$

1: **Define search area and grid of candidate positions**
2: **Building Boundaries (BB) computation**
For each candidate position, predict building edges using the 3D city model
3: **Predict satellite visibility**
For each candidate position, predict satellite visibility using the Building Boundaries information
4: **Measure satellite visibility**
Use C/N0 ratios to determine the observed satellite visibility
5: **Scoring of candidate positions**
Based on matching between predicted and measured satellite visibility, score each candidate point
6: **Final position estimation**
Estimate the final user position based on weighting of position having the highest scores

In this experimentation, we have used our implementation of Shadow Matching solution to compare and assess the performance of our proposed algorithm. Shadow Matching algorithm have been implemented using GPS and GLONASS signals. Our proposed AML-3D have been implemented using GPS signals only since 3D GNSS simulation using GLONASS constellation is not yet optimized in the current version of the simulator.

D. Performances of the Proposed Solution

For this validation test, we have compared the positioning performance using AML-3D solution without 3D simulation error correction, i.e. $\delta_{3D} = 0$, Shadow-Matching solution (SM-3D), the UBLOX receiver solution, a SEPTENTRIO receiver solution, and a conventional Least-Squares solution. Fig. 5 shows the cumulative distribution function of the horizontal position errors of the proposed AML-3D solution, Shadow-Matching solution (SM-3D) and the conventional solution in the considered scenario.

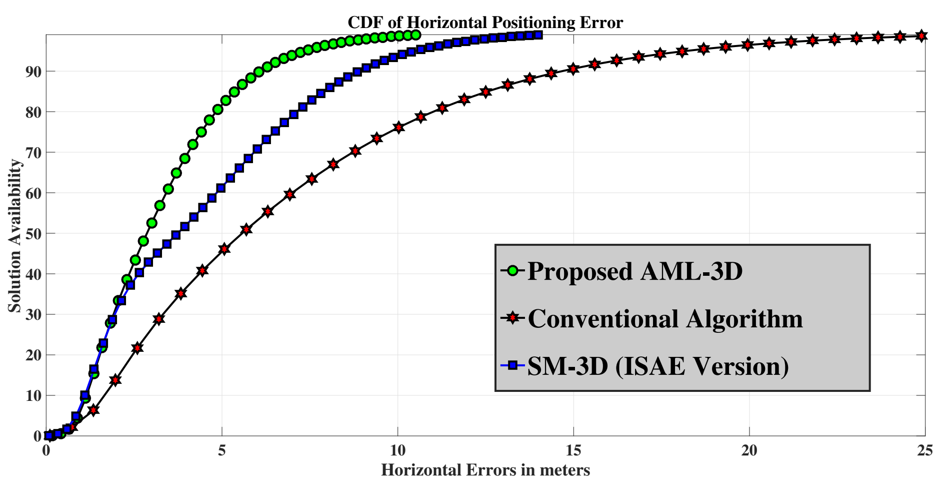

Fig. 5: CDF of Horizontal Positioning Errors

It is apparent from the CDF figure in Fig. 5 that our approach AML-3D gives more positioning performance compared to the conventional GNSS solution. AML-3D positioning performance in this scenario is comparable to that of the Shadow-Matching solution (SM-3D: ISAE Version). We compare horizontal positioning errors (HPE) for these estimators in this scenario. Results are shown in Table I. We notice that AML-3D outperforms, in average, all solutions even the very accurate and stable SEPTENTRIO solution.

TABLE I: HORIZONTAL POSITIONING PERFORMANCES

	AML-3D	SM-3D	SEPTENTRIO	UBLOX	Conventional Algorithm
Mean of HPE [m]	3.18	4.22	4.25	7.27	6.6
HPE at 95% [m]	5.86	7.95	4.5	11.65	14.66
HPE at 97% [m]	6.66	9.15	4.52	11.85	15.78
HPE at 99% [m]	9.18	9.56	4.57	12.41	18.32

The scoring map of the proposed AML-3D solution and the different solution for a fixed time epoch is shown in Fig. 6.

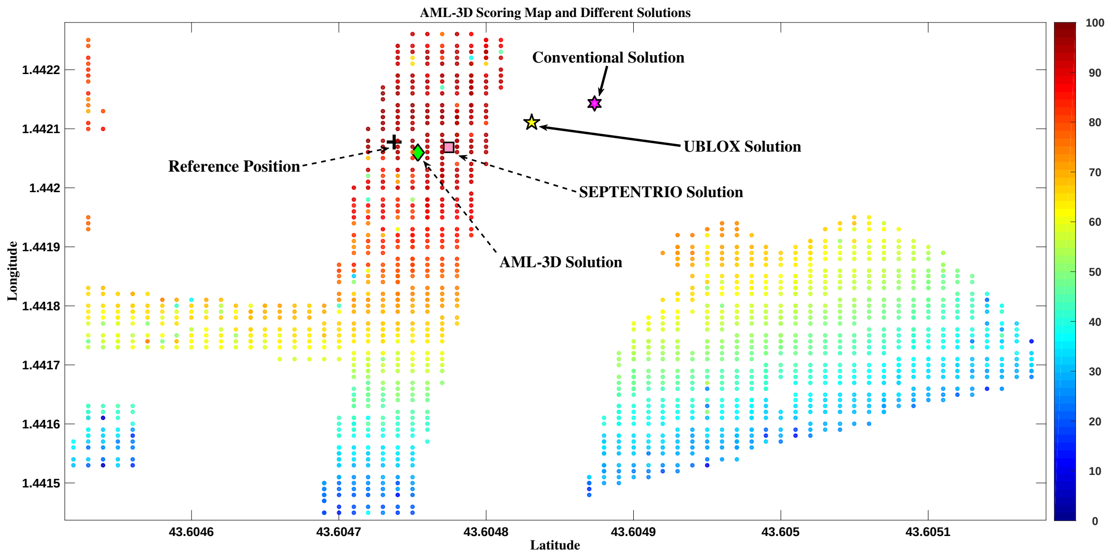

Fig. 6: AML-3D scoring map with different estimation solution for a fixed time epoch

The previous example illustrates the effectiveness of the proposed AML-3D algorithm even in degraded conditions. Positioning performance of the AML-3D estimator exceed that of receiver solutions (very good and reliable positioning solutions in general). Taken into account that the 3D simulator SPRING is continuously improved by CNES, these performance obtained by AML-3D might reach optimal positioning performance even in presence in MP/NLOS biases.

Despite this performance enhancement, the proposed approach is computationally intensive because of bias estimation using the 3D GNSS simulator. Nevertheless, this method can be easily implemented on a server mode and send the 3D biases to the mobile receiver to compute its position.

E. Sensitivity Analysis of Parameters

1) 3D PR bias Prediction Error:

We improve the proposed technique by modeling the uncertainty on the bias prediction by 3D GNSS simulations. In fact, the performance of this proposed method is strongly linked to the performances of PR bias prediction using 3D simulation. One of the greatest challenges is that generally these biases are environment-dependent and highly time-varying and hence very difficult to be estimated.

In this study, we attempt to model this bias prediction inaccuracy using different criterion. We propose two ways to correct the error of PR bias prediction by 3D simulation: 3D bias uncertainty correction based on satellite elevation angles (12) and 3D bias uncertainty correction based on the C/N0 ratios (13). Horizontal positioning performance of different estimator with correction of the 3D PR bias prediction error are given in Fig. 7 and in Table II. We compare the positioning performance of AML-3D algorithm without 3D bias uncertainty correction $\delta_{3D} = 0$, the AML-3D algorithm with the 3D bias uncertainty correction (12) and the AML-3D algorithm with the 3D bias uncertainty correction (13).

We note performance enhancement by modeling the 3D simulation uncertainty either with (12) or (13). In this considered scenario, the 3D bias uncertainty model based on elevation angle is given better positioning accuracy compared the 3D bias uncertainty based on the C/N0.

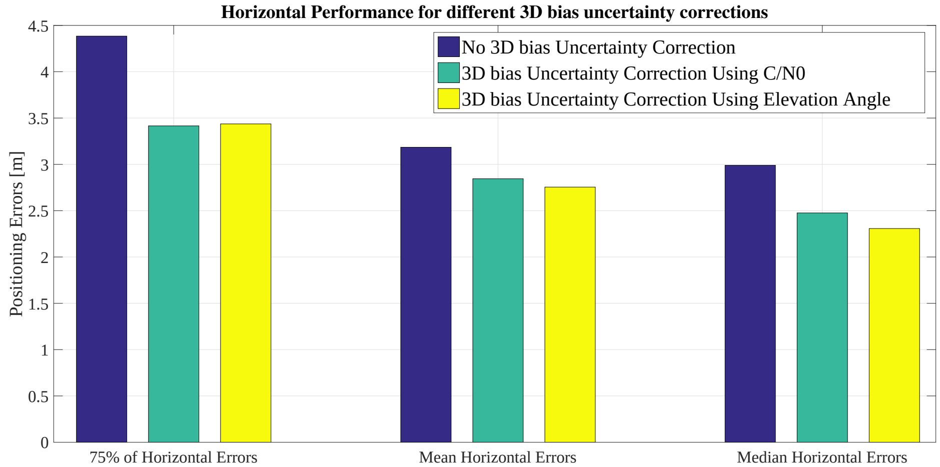

Fig. 7: Positioning Performance with 3D bias Uncertainty correction

TABLE II: HORIZONTAL POSITIONING PERFORMANCES

	AML-3D with $\delta_{3D} = 0$	**AML-3D** with $\delta_{3D} \sim (12)$	**AML-3D** with $\delta_{3D} \sim (13)$
H-RMSE [m]	3.18	2.75	2.84
HPE at 95% [m]	5.86	5.34	5.32

2) Effect of Grid Size:

Another important parameter used the proposed AML-3D method is the selection of the array of candidate positions. In this subsection, we propose an analysis on the effect of the size of the grid of candidate positions on the performance of the proposed AML-3D method. To do this, we vary the number of the considered candidate positions, while always ensuring that the considered grid of candidate positions is centred on the reference solution. Fig. 8 shows the variation of the mean, median and maximum horizontal positioning errors of the AML-3D algorithm without 3D simulation uncertainty correction $\delta_{3D} = 0$ with respect to the number of candidate positions.

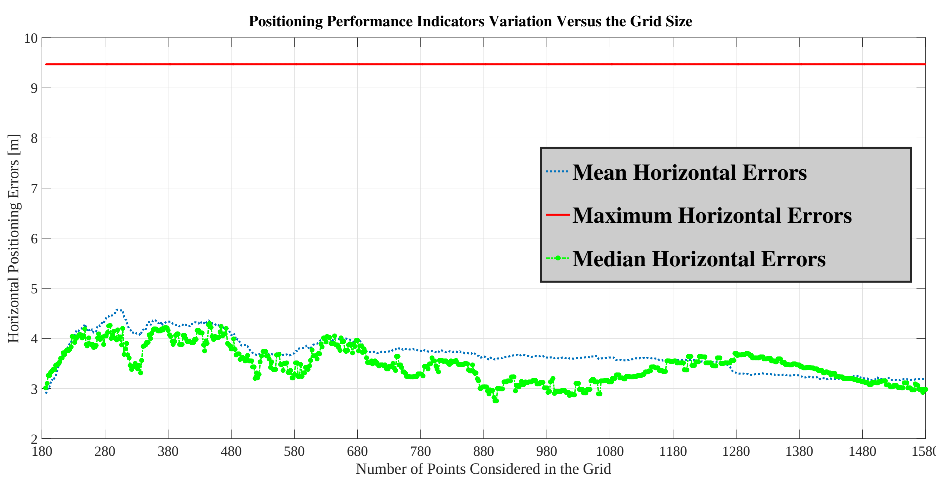

Fig. 8: Positioning Performance Versus the size of the considered grid of positions

We note that the positioning performance of the proposed AML-3D algorithm remains almost at the same accuracy level when varying the number of positions in the considered array of candidate locations. The positioning errors are also bounded independently of the size of the grid of candidate positions.

This obtained result shows that the proposed method is not highly dependant on the size of the array of candidate positions as far as the central region of candidate positions is close to the true position. This is explained by the fact that high matching scores are always in this central region and very low matching scores are obtained in the other regions. As the final solution is obtained by weighting of the candidate positions with the highest scores, then the final estimation will remain almost the same independently on the size of the used grid of points.

3) Reference Satellite Selection:

In the proposed AML-3D method, we eliminate the receiver clock bias from the problem estimation by differentiation of all ranging measurements across satellites using a reference satellite. Hence, the selection of reference satellite is a quite important step. This reference satellite must verify the following: the pseudorange measurements of this satellite must be reliable and almost clean, i.e. containing very low PR measurements errors. Basic indicators for this selection process include elevation angle and C/N0 values. LOS probability indicator is proposed in [29]. This LOS probability is computed using signal power distributions and some tuning parameters fixed using experimental data. The LOS probility can be expressed as:

$$P_{LOS} = \ln \frac{p_{LOS}(C/N_0|\mathbf{Elev})}{p_{NLOS}(C/N_0|\mathbf{Elev})}$$

Where P_{LOS} is the LOS probability for a considered satellite, $p_{LOS}(C/N_0|\mathbf{Elev})$ and $p_{NLOS}(C/N_0|\mathbf{Elev})$ are the signal power distributions of LOS and NLOS satellites, which depend on fixed tuning parameters. Further details about this LOS probability computation may be obtained in [29].

In this subsection, different indicators for this selection process are evaluated and compared. We evaluate the positioning accuracy of the AML-3D algorithm with different selection criteria: satellite elevation, C/N0 and LOS probability indicators. Obtained results are shown in Fig. 9.

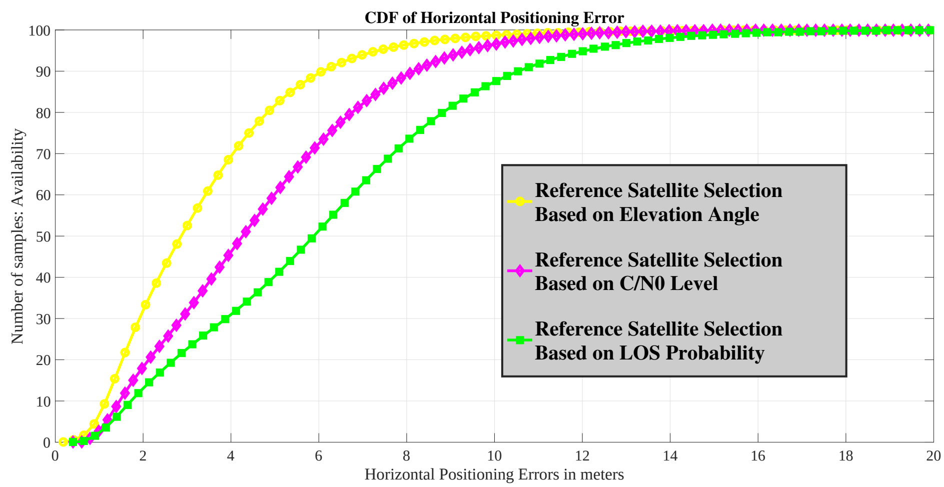

Fig. 9: CDF of Horizontal Errors for different Reference Satellite Selection methods

Mean of horizontal positioning errors in these different cases are compared in the following Table III.

TABLE III: HORIZONTAL POSITIONING PERFORMANCES

	Selection Based on Elevation Angle	**Selection Based on C/N0**	**Selection Based on LOS Probability**
H-RMSE [m]	3.18	4.46	5.91

This analysis shows that the satellite elevation angle indicator gives the best positioning performance. This result is explained by the fact that during this measurements campaign the GPS satellite (G15) had a very high elevation angle (around 80° as shown in Fig. 2. This satellite was then received all the time in line-of-sight and hence PR measurements from G15 are always reliable. With other measurements set, the obtained conclusions may be different. Finally, the LOS probability indicator is giving low positioning accuracy compared to other indicators because this indicator depends highly on parameters set in advance and is therefore not always reliable.

V. Conclusion

Much of the previous research has focused on NLOS mitigation for positioning performance enhancement. But, a new trend of studies highlights the need for NLOS constructive use by ranging biases correction instead of simple mitigation. In this regard, this research sheds new lights on PR bias constructive use by use of a 3D GNSS simulator. The proposed idea is based on position estimation among an array of candidate positions by approximate likelihood scoring. The scoring of each candidate position is performed using a ranging measurement matching criterion based on a 3D bias estimated using a 3D GNSS simulator. The key strength of this approach is its sub-optimal effectiveness, which was been proven theoretically and using real GNSS data. Notwithstanding the significant computational loads, this approach offers valuable insights into precise GNSS positioning in presence of MP/NLOS receptions.

In terms of directions for future research, further works could focus on enhancing the propagation simulation to reach a higher positioning performance using our approach. Finally, the permanent advancement made on environment modeling would help us to achieve higher accuracy using this approach. In this perspective, testing this approach in different environments would be a fruitful area for further work.

Acknowledgements

The authors would like to thank the French Space Agency (CNES) for funding this research project: SPRING Usage for Modeling Multipath Effects on a Receiver (SUMMER). We would like also to thank UCL Engineering's Space Geodesy and Navigation Laboratory (SGNL) for their kind support with problems related to 3D modeling.

APPENDIX A

We start by computing the expression of $\hat{\mathbf{x}}_{AML}$:

$$\hat{\mathbf{x}}_{AML} = \underset{\mathbf{x}_i}{\operatorname{argmin}}\{\frac{\partial}{\partial \mathbf{x}_i}(\Pi(\mathbf{y}|\mathbf{x}_i, \mathbf{b}_{3D}(\mathbf{x}_i)) = 0)\}$$

We compute the derivative of the cost function:

$$\frac{\partial}{\partial \mathbf{x}_i}(\Pi(\mathbf{y}|\mathbf{x}_i, \mathbf{b}_{3D}(\mathbf{x}_i))) = -2(\mathbf{H}_0^\top + \frac{\partial}{\partial \mathbf{x}_i}\mathbf{b}_{3D}(\mathbf{x}_i))\mathbf{R}^{-1}\mathbf{G}(\mathbf{x}_i)$$

Where $\mathbf{G}(\mathbf{x}_i) = \mathbf{y} - \mathbf{H}_0\mathbf{x}_i - \mathbf{b}_{3D}(\mathbf{x}_i)$. Then, we get the following expression for the approximate maximum likelihood:

$$\mathbf{y} - \mathbf{H}_0\hat{\mathbf{x}}_{AML} - \mathbf{b}_{3D}(\hat{\mathbf{x}}_{AML}) = 0$$

Since the MSE matrix is diagonal, the overall mean square error of the AML estimation is expressed as:

$$\mathrm{Tr}\{MSE[\hat{\mathbf{x}}_{AML}]\} = \mathrm{Tr}\{E[(\hat{\mathbf{x}}_{AML} - \mathbf{x})(\hat{\mathbf{x}}_{AML} - \mathbf{x})^\top]\} = E[\|\hat{\mathbf{x}}_{AML} - \mathbf{x}\|_2^2]$$

The AML estimation error can be expressed as:

$$\|\hat{\mathbf{x}}_{AML} - \mathbf{x}\|_2^2 = \|\mathbf{H}_0^+(\mathbf{H}_0\hat{\mathbf{x}}_{AML} - \mathbf{H}_0\mathbf{x})\|_2^2 = \|\mathbf{H}_0^+(\mathbf{b} - \mathbf{b}_{3D}(\hat{\mathbf{x}}_{AML}) + \mathbf{v})\|_2^2$$

The previous expression gives:

$$\mathrm{Tr}\{MSE[\hat{\mathbf{x}}_{AML}]\} \leq E\{\|\mathbf{H}_0^+(\mathbf{b} - \mathbf{b}_{3D}(\hat{\mathbf{x}}_{AML}))\|_2^2\} + E\{\|\mathbf{H}_0^+\mathbf{v}\|_2^2\}$$

By developing the two parts of this inequality, we show that:

$$E[\|\mathbf{H}_0^+\mathbf{v}\|_2^2] = \mathrm{Tr}\{(\mathbf{H}_0^\top\mathbf{R}^{-1}\mathbf{H}_0)^{-1}\} = \mathrm{Tr}\{MSE[\hat{\mathbf{x}}_{ML}]\}$$

$$E[\|\mathbf{H}_0^+(\mathbf{b} - \mathbf{b}_{3D}(\hat{\mathbf{x}}_{AML}))\|_2^2] = \mathrm{Tr}\{(\mathbf{H}_0^+E[\delta_{3D}^{AML}(\delta_{3D}^{AML})^\top](\mathbf{H}_0^+)^\top)\}$$

Where $\delta_{3D}^{AML} = \mathbf{b} - \mathbf{b}_{3D}(\hat{\mathbf{x}}_{AML})$. Besides, we have the following inequality for all candidate positions:

$$\|\mathbf{b} - \mathbf{b}_{3D}(\mathbf{x}_i)\|_{\mathbf{R}^{-1}}^2 \leq \|\mathbf{b} - \mathbf{b}_{3D}(\mathbf{x})\|_{\mathbf{R}^{-1}}^2 + \|\mathbf{b}_{3D}(\mathbf{x}_i) - \mathbf{b}_{3D}(\mathbf{x})\|_{\mathbf{R}^{-1}}^2$$

And then, we deduce that:

$$\|\delta_{3D}^{AML}\|_{\mathbf{R}^{-1}}^2 = \min_{\mathbf{x}_i}\|\mathbf{b} - \mathbf{b}_{3D}(\mathbf{x}_i)\|_{\mathbf{R}^{-1}}^2 \leq \delta_{3D} + \min_{\mathbf{x}_i}\|\mathbf{b}_{3D}(\mathbf{x}_i) - \mathbf{b}_{3D}(\mathbf{x})\|_{\mathbf{R}^{-1}}^2 \leq (1+\eta)\delta_{3D}$$

where $\eta \ll 1$ and then lemma 2 is proven.

APPENDIX B

We start from the following relation for the AML solution:

$$\mathbf{y} - \mathbf{H}_0\hat{\mathbf{x}}_{AML} - \mathbf{b}_{3D}(\hat{\mathbf{x}}_{AML}) = 0$$

Let us compute the AML and ML solutions difference, which can be expressed as:

$$\|\hat{\mathbf{x}}_{AML} - \hat{\mathbf{x}}_{ML}\|_2^2 = \|\mathbf{H}_0^+(\mathbf{H}_0\hat{\mathbf{x}}_{AML} - \mathbf{y} + \mathbf{b})\|_2^2 = \|\mathbf{H}_0^+(\mathbf{b} - \mathbf{b}_{3D}(\hat{\mathbf{x}}_{AML}))\|_2^2$$

By definition of the operator norm of matrix $\mathbf{H}_0^+$:

$$\|\hat{\mathbf{x}}_{AML} - \hat{\mathbf{x}}_{ML}\|_2^2 \leq \|\mathbf{R}^{-1/2}\mathbf{H}_0^+\|_F^2\|\mathbf{b} - \mathbf{b}_{3D}(\hat{\mathbf{x}}_{AML})\|_2^2$$

Where, we define the Frobenius matrix norm as:

$$\|\mathbf{R}^{-1/2}\mathbf{H}_0^+\|_F = \mathrm{Tr}\{(\mathbf{H}_0^+)^\top\mathbf{R}^{-1}\mathbf{H}_0^+\} = \mathrm{Tr}\{\mathbf{R}^{-1/2}\mathbf{H}_0^+(\mathbf{H}_0^+)^\top\mathbf{R}^{-1/2}\}$$

Since matrix $\mathbf{R}$ is diagonal with equal diagonal elements:

$$\|\mathbf{R}^{-1/2}\mathbf{H}_0^+\|_F = \mathrm{Tr}\{\mathbf{R}^{-2}(\mathbf{H}_0^\top\mathbf{R}^{-1}\mathbf{H}_0)^{-1}\}$$

Matrices in the trace operator are matrices with positive diagonal elements. Then, we get the following inequality:

$$\mathrm{Tr}\{\mathbf{R}^{-2}(\mathbf{H}_0^\top\mathbf{R}^{-1}\mathbf{H}_0)^{-1}\} \leq \mathrm{Tr}\{\mathbf{R}^{-2}\}\mathrm{Tr}\{(\mathbf{H}_0^\top\mathbf{R}^{-1}\mathbf{H}_0)^{-1}\}$$

The second term can be expressed as:

$$\mathrm{Tr}\{\mathbf{R}^{-2}\}\mathrm{Tr}\{(\mathbf{H}_0^\top\mathbf{R}^{-1}\mathbf{H}_0)^{-1}\} = \frac{N \times \mathrm{Tr}\{\mathbf{DOP}\}}{\sigma^2} = \frac{N \times GDOP}{\sigma^2}$$

Where $\mathbf{DOP} = (\mathbf{H}_0^\top\mathbf{H}_0)^{-1}$ is the Dilution of Precision (DOP) matrix, $GDOP$ is the Geometric Dilution Of Precision, N is the number of received GNSS signals and σ are the diagonal values of the noise covariance matrix, i.e $\mathbf{R} = \sigma\mathbf{I}$. Finally, using the previous appendix, we have shown that:

$$\|\mathbf{b} - \mathbf{b}_{3D}(\hat{\mathbf{x}}_{AML})\|_{\mathbf{R}^{-1}}^2 \leq (1+\eta)\delta_{3D}$$

This proves lemma 3.

REFERENCES

[1] GSA, "GNSS Market Report Issue 5," GSA, Tech. Rep., May, 2017.

[2] P. Groves, "Multipath vs. NLOS signals. How Does Non-Line-of-Sight Reception Differ from Multipath Interference," *Inside GNSS 2013*.

[3] L. Wang, P. D. Groves, and M. K. Ziebart, "GNSS shadow matching: Improving urban positioning accuracy using a 3D city model with optimized visibility scoring scheme," *Navigation*, vol. 60, no. 3, pp. 195–207, 2013.

[4] P. D. Groves, Z. Jiang, L. Wang, and M. K. Ziebart, "Intelligent Urban Positioning using Multi-Constellation GNSS with 3D Mapping and NLOS Signal Detection," in *Proc. of ION GNSS 2012*, no. 458 - 472.

[5] P. D. Groves and Z. Jiang, "Height Aiding, C/N0 Weighting and Consistency Checking for GNSS NLOS and Multipath Mitigation in Urban Areas," *Journal of Navigation*, pp. 653–659, 2013.

[6] S. Peyraud, D. Bétaille, S. Renault, M. Ortiz, F. Mougel, D. Meizel, and F. Peyret, "About non-line-of-sight satellite detection and exclusion in a 3D map-aided localization algorithm," *Sensors*, vol. 13, no. 1.

[7] J. Marais, S. Tay, A. Flancquart, and C. Meurie, "Weighting with the pre-knowledge of GNSS signal state of reception in urban areas," in *Proceedings of ENC 2015*.

[8] A. Bourdeau, M. Sahmoudi, and J.-Y. Tourneret, "Constructive use of GNSS NLOS-multipath: Augmenting the navigation Kalman filter with a 3D model of the environment," in *Proc. of FUSION 2012*. IEEE.

[9] M. S. Braasch, "Performance comparison of multipath mitigating receiver architectures," in *Proc. IEEE Aerospace Conference*, vol. 3, 2001.

[10] L. Garin and J. Rousseau, "Enhanced Strobe Correlator Multipath Rejection for Code & Carrier ," in *Proceedings of the 10th International Technical Meeting of the Satellite Division of The Institute of Navigation (ION GPS 1997)*, Kansas City, MO, Sep. 1996, pp. 657–664.

[11] R. D. Van Nee, J. Siereveld, P. C. Fenton, and B. R. Townsend, "The multipath estimating delay lock loop: approaching theoretical accuracy limits," in *Position Location and Navigation Symposium, 1994., IEEE*, 1994, pp. 246–251.

[12] M. Sahmoudi and R. J. Landry, "Multipath Mitigation Techniques using Maximum-Likelihood Principles," *Inside GNSS 2008*.

[13] I. Guvenc and C. C. Chong, "A Survey on TOA Based Wireless Localization and NLOS Mitigation Techniques," *IEEE Communications Surveys Tutorials*, vol. 11, no. 3, pp. 107–124, rd 2009.

[14] P. Petrus, "Robust Huber adaptive filter," *IEEE Transactions on Signal Processing*, vol. 47, no. 4, pp. 1129–1133, 1999.

[15] K. Fallahi, C.-T. Cheng, and M. Fattouche, "Robust positioning systems in the presence of outliers under weak GPS signal conditions," *IEEE Systems Journal*, vol. 6, no. 3, pp. 401–413, 2012.

[16] A. Rabaoui, N. Viandier, E. Duflos, J. Marais, and P. Vanheeghe, "Dirichlet Process Mixtures for Density Estimation in Dynamic Nonlinear Modeling: Application to GPS Positioning in Urban Canyons," *IEEE Transactions on Signal Processing*, vol. 60, no. 4, 2012.

[17] M. A. Quddus, W. Y. Ochieng, and R. B. Noland, "Current map-matching algorithms for transport applications: State-of-the art and future research directions," *Transportation Research Part C: Emerging Technologies*, vol. 15, no. 5, pp. 312 – 328, 2007.

[18] N. Kbayer, M. Sahmoudi, and E. Chaumette, "Robust GNSS Navigation in Urban Environments by Bounding NLOS Bias of GNSS Pseudoranges Using a 3D City Model ," in *Proceedings of ION GNSS+ 2015*.

[19] Y. Ng and G. X. Gao, "Direct Position Estimation Utilizing Non-Line-of-Sight (NLOS) GPS Signals," in *Proceedings of the 29th International Technical Meeting of The Satellite Division of the Institute of Navigation (ION GNSS+ 2016)*.

[20] M. Adjrad and P. D. Groves, "Intelligent Urban Positioning using Shadow Matching and GNSS Ranging aided by 3D Mapping," in *Proceedings of ION GNSS+*, Portland, September 2016.

[21] R. Kumar and M. G. Petovello, "A novel GNSS positioning technique for improved accuracy in urban canyon scenarios using 3D city model," in *Proc. of ION GNSS+ 2014, Tampa, FL, USA*, vol. 812.

[22] T. Suzuki and N. Kubo, "Correcting GNSS multipath errors using a 3D surface model and particle filter," *Proc. ION GNSS+ 2013*.

[23] S. Miura, S. Hisaka, and S. Kamijo, "GPS multipath detection and rectification using 3D maps," in *Proc. of IEEE ITSC 2013*.

[24] D. Betaille, F. Peyret, M. Ortiz, S. Miquel, and L. Fontenay, "A new modeling based on urban trenches to improve GNSS positioning quality of service in cities," *IEEE Intelligent Transportation Systems Magazine*.

[25] N. Kbayer and M. Sahmoudi, "Constructive Use of MP/NLOS bias of GNSS Pseudoranges: Performance Analysis by Type of Environment," in *Proc. of ION ITM 2017*.

[26] T. Chapuis, B. Bonhoure, F. Lacoste, C. Boulanger, D. Lapeyre, K. Urbanska, P. Noirat, and A. Marion, "SPRING simulator A powerful 3D computing engine toward urban canyons modelling," in *Satellite Navigation Technologies and European Workshop on GNSS Signals and Signal Processing,(NAVITEC), 2012 6th ESA Workshop on*. IEEE, 2012, pp. 1–8.

[27] P. Misra and P. Enge, *Global Positioning System: Signals, Measurements, and Performance*, 2nd ed. Ganga-Jamuna Press, Lincoln MA, 2006.

[28] S. M. Kay, *Fundamentals of statistical signal processing, volume I: estimation theory*. Prentice Hall, 1993.

[29] T. Iwase, N. Suzuki, and Y. Watanabe, "Estimation and exclusion of multipath range error for robust positioning," *GPS solutions 2013*.

[30] P. D. Groves, "Shadow Matching: A New GNSS Positioning Technique for Urban Canyons," *Journal of Navigation*, vol. 64, no. 3, 2011.

[31] A. Irish, J. Isaacs, D. Iland, J. Hespanha, E. Belding, and U. Madhow, "Demo: ShadowMaps, the urban phone tracking system," in *Proceedings of the 20th annual international conference on Mobile computing and networking*. ACM, 2014, pp. 283–286.

[32] L. Wang, P. D. Groves, and M. K. Ziebart, "Urban positioning on a smartphone: Real-time shadow matching using GNSS and 3D city models." The Institute of Navigation, 2013.